RAA 2019 Vol. **19** No. **10**, 142(8pp) doi: 10.1088/1674–4527/19/10/142

http://www.raa-journal.org *http://iopscience.iop.org/raa*

***R**esearch in*
***A**stronomy and*
***A**strophysics*

Simultaneous optical g, r, i monitoring and IDV periodic analysis for quasar 3C 454.3

Jun-Hui Fan[1,2], Yu-Hai Yuan[1,2], Hong Wu[3], Feng Wang[1,2], Jun Tao[4,5] and Min-Feng Gu[5]

[1] Center for Astrophysics, Guangzhou University, Guangzhou 510006, China; *fjh@gzhu.edu.cn*
[2] Astronomy Science and Technology Research Laboratory of Department of Education of Guangdong Province, Guangzhou 510006, China
[3] Key Laboratory of Optical Astronomy, National Astronomical Observatories, Chinese Academy of Sciences, Beijing 100101, China
[4] Shanghai Astronomical Observatory, Chinese Academy of Sciences, Shanghai 200030, China
[5] Key Laboratory for Research in Galaxies and Cosmology, Shanghai Astronomical Observatory, Chinese Academy of Sciences, Shanghai 200030, China

Received 2019 March 13; accepted 2019 May 6

Abstract With the 1.26 m National Astronomical Observatory-Guangzhou University Infrared/Optical Telescope (NAGIOT) at Xinglong Station of National Astronomical Observatories, Chinese Academy of Sciences, we obtained 419 groups of simultaneous observations at g, r and i bands, for the first time, targeting quasar 3C 454.3 during 15 nights from 2016 October 23 to 2016 December 15. Based on our observations, we investigate the optical variabilities, the relation between brightness and color index, and the periodicity variability. The presented analyses demonstrate that: 1. The maximum variations at the g, r and i bands are $\Delta m_{g|\max} = 1.015 \pm 0.042$ mag, $\Delta m_{r|\max} = 1.188 \pm 0.050$ mag and $\Delta m_{i|\max} = 1.305 \pm 0.057$ mag respectively. 2. During our 15 night monitoring program, intra-day variability was detected on one night (Nov. 2). Also, the brightness increased by $A = 15.86\%$ over 50.8 min, then decreased by $A = 22.42\%$ over 40.1 min. After a small bright state, its brightness increased again by 18.1% over 55 min at the g band. Similar phenomena happened at r and i bands. The intra-day variabilities at the three bands on 2016 November 2 indicate a period of 105 min, which implies a black hole mass of $M_{\rm BH} = (0.3 \sim 1.85) \times 10^9\, M_\odot$. 3. There is an anti-correlation between color index and magnitude, suggesting the source becomes redder when it brightens.

Key words: galaxies: quasars: individual (3C 454.3)

1 INTRODUCTION

Blazars manifest extreme observation properties, such as violent optical variability, high and variable polarization, superluminal motion, highly energetic emissions and so on. These properties are characterized by the jet along our line of sight (Angel & Stockman 1980; Blandford & Rees 1978; Urry & Padovani 1995; Ackermann et al. 2015; Fan et al. 2016, 2017a,b, 2018a; ; Liu et al. 2017; Xiong et al. 2017; Meng et al. 2018; Yang et al. 2018a,b; Pei et al. 2019; Rieger 2019; Xiao et al. 2019 and reference therein). Up to now, TeV sources are almost all identified as blazars (Lin & Fan 2018).

Blazars can be divided into two subclasses, BL Lacetae objects (BL Lacs) and flat spectrum radio quasars (FSRQs). FSRQs show strong broad emission lines (Urry & Padovani 1995) while BL Lacs are characterized by absent or very weak emission lines (Stickel et al. 1991). The two subclasses are separated by the equivalent width (EW) of their optical emission lines. Generally BL Lacs display EW$<$ 5 Å (Urry & Padovani 1995; Ghisellini et al. 2011; Sbarrato et al. 2012; Ghisellini & Tavecchio 2015).

Blazars exhibit violent optical variabilities. Study of their variability is important for understanding the nature and emission properties of blazars. From the variations, we can ascertain different timescales ranging from minutes to years, which can be divided into three types: intra-day variability (IDV) with timescale of one day or less, short-term variations (STV) with a timescale of days to months and long-term variations (LTV) with timescale of years (Fan 2005). IDV is usually non-periodic, and might come from the jets, instability of accretion disc, or the interstellar medium and so on. There are many theoretical models used to explain these variations, for example, shocks

propagating along the relativistic jets (Marscher & Gear 1985; Wagner & Witzel 1995), or hotspots or disturbances on or above accretion discs surrounding the black holes (Chakrabarti & Wiita 1993; Mangalam & Wiita 1993).

For observations, Romero et al. (1999) (see also Cellone et al. 2000 and Fan et al. 2001) introduced a variability parameter, $C_i = \frac{\sigma_{(O-S_i)}}{\sigma_{(S_1-S_2)}}$, $i = 1$ and 2, to check the reality of such variability. Here, $\sigma_{(O-S_i)}$ is the deviation of measured values between the target object and the comparison star, and $\sigma_{(S_1-S_2)}$ is the deviation from two comparison stars. If $C(= \frac{C_1+C_2}{2})$, the average value of C_1 and C_2, is greater than 2.576, then the nominal confidence level of a variability detection is greater than 99%. However, this criterion is usually too conservative because it is not appropriately distributed. de Diego (2010) discussed an F-test to verify that such variability is real. The F-test is derived from statistical theory, and the related F statistics (F-test and ANOVA) are based on noncentral F distributions (de Diego 2014; de Diego et al. 2015, see also Gaur et al. 2012; Xiong et al. 2017; Fan et al. 2018a; Zhang et al. 2018; Pandey et al. 2019).

In Heidt & Wagner (1996) introduced a variability amplitude parameter, A_m for variability,

$$A_m = 100 \times \sqrt{(m_{\max} - m_{\min})^2 - {\sigma_{\max}}^2 - {\sigma_{\min}}^2}(\%).$$

Here, $m_{\min}$ and $m_{\max}$ are the minimum and maximum magnitudes respectively, and $\sigma_{\min}$ and $\sigma_{\max}$ are the corresponding uncertainties.

So, if $C \geq 2.576$ and the F-test value is higher than the critical value (see Fan et al. 2018a), we can obtain the corresponding variability parameter A_m and take the corresponding interval as the timescale, ΔT.

We also introduce the following method to constrain short-term optical variability. For any two pairs of observations $S_j(t_j, m_j)$, $S_k(t_k, m_k)$ $(j, k = 1, 2, ...N)$, we calculate three parameters, time interval: $\Delta t_{jk} = |t_j - t_k|$, magnitude difference: $\Delta m_{jk} = |m_j - m_k|$ and standard deviation: $\sigma_{jk} = \sqrt{{\sigma_j}^2 + {\sigma_k}^2}$. If $\Delta m_{jk} > 3\sigma_{jk}$, then we take Δm_{jk} as a real variation and the corresponding time interval Δt_{jk} as the timescale. If there are more cases with $\Delta m_{jk} > 3\sigma_{jk}$, then we regard the shortest Δt_{jk} as the timescale as we did in our former papers (Fan et al. 2009a,b,c, 2014).

3C 454.3 (PKS 2251+158), located at $z = 0.859$ (Jackson & Browne 1991), is a quasar. It is nicknamed the "Crazy Diamond" by the *AGILE* team (Vercellone et al. 2010) and is one of the brightest blazars ever identified. It exhibits strong variability over all electromagnetic bands (Bennett 1962; Bennett et al. 2003; Sandage 1966; Worrall et al. 1987; Hartman et al. 1993, 1999; Blom et al. 1995; Raiteri et al. 1998; Tavecchio et al. 2002; Zhang et al. 2005; Jorstad et al. 2013; Britto et al. 2016; Gupta et al. 2017; Kushwaha et al. 2017 and references therein). The maximum variation is $\Delta \mathrm{m} = 2.3$ (Angel & Stockman 1980), and a variability of 0.5 mag over a timescale of one day was reported by Lloyd (1984). During our monitoring period of Oct. 2000 carried out with the 70 cm telescope at Abastumani Observatory, Georgia, it did not show any clear variability (Fan et al. 2004). 3C 454.3 brightened in 2001 and in 2005, reaching its brightest value ever observed in the optical band with $R = 12.0$ mag (Villata et al. 2006; Giommi et al. 2006; Pian et al. 2006; Fuhrmann et al. 2006). Gaur et al. (2012) analyzed its observations during 2009 and 2010, and found IDVs in four nights. Based on a multiwavelength spectral model, Bonnoli et al. (2011) estimated its Doppler factor of $\delta \sim 25$ during an outburst. It is also the target in our monitoring programs at Shanghai Astronomical Observatory and Abastumani Observatory (Fan et al. 2004, 2014, 2017a; Kurtanidze et al. 2009; Tao et al. 2008) and at Xinglong Station of National Astronomical Observatories, Chinese Academy of Sciences (NAOC).

This paper is arranged as follows. In Section 2, we present the observations and data reductions. In Section 3, we describe the analysis methods and results. Finally in Section 4, we will discuss the results and draw our conclusions.

2 OBSERVATIONS AND DATA REDUCTIONS

2.1 Photometry Process

The observations were simultaneously carried out at g, r and i bands on the 1.26-m National Astronomical Observatory-Guangzhou University Infrared/Optical Telescope (NAGIOT) at Xinglong Station of National Astronomical Observatories, Chinese Academy of Sciences (NAOC). Since 2014, a new optical system was designed and installed to split the optical beam into optical and near infrared channels. The optical beam is further split into three optical passbands by the TRIPOL5 instrument and the infrared beam is redirected into the PSL camera. Thus, the system enables simultaneous photometry in three optical bands and one infrared band. Unfortunately, the near infrared camera did not work well until now. TRIPOL5 uses three SBIG STT-8300M cameras, each with a CCD of size 3326×2504 pixels and field of view of $6.0' \times 4.5'$. The filters adopt standard SDSS g, r, i bands.

Bias images were taken at the beginning and end of the corresponding night observation. The flat-field images were recorded at dusk and dawn. For the target, the exposure time was 300 seconds.

2.2 Data Reductions

All of the observational data have been reduced by a data reduction system which has been deployed on a cloud environment. After referring to a similar system (Mommert 2017), we designed a fully automatic photometry pipeline

for NAGIOT. The codes for the system were written in the Python language. Meanwhile, two classical photometry software packages (Bertin & Arnouts 1996), i.e., SExtractor and SCAMP, were also integrated into the system.

We chose *Gaia* (Gaia Collaboration et al. 2016) as the astrometry catalog and SDSS (Ahn et al. 2012) as the photometry catalog while processing the data. Considering the observational targets in the study, SDSS would be the best choice because it can directly provide $ugriz$ magnitudes.

The data reduction is fully automatic. The reduction procedure can be divided into four steps.

1) FITS header supplement. At the beginning, the header of the FITS files was supplemented according to the observation log. Some important fields, such as OBJECTS, RA, DEC, exposure time and so on, were added. Based on these fields, SExtractor extracted all possible stars from the FITS files.

2) Coordinate Matching. According to the positions of the possible stars, SCAMP will match these coordinates with the *Gaia* catalog so as to determine the telescope pointing accurately.

3) Aperture size. We finally use the growth curve method to obtain the appropriate aperture because the IRAF apphot package ignores the effects of atmospheric jitter and produces a bigger aperture than the growth curve method.

4) Photometry. The photometry pipeline uses the magnitudes of at least three standard stars from the SDSS-R9 star catalog to calculate the zero-point magnitude for each FITS file and then outputs the real magnitude of the observed object and other standard stars. During data reduction, at least one of the standard stars would be chosen as the control star to monitor the photometry stability and quality of the data processing.

We finally verify the correctness of the final results. We reduced some data by using both the IRAF Apphot package and the pipeline. The results indicate that the two software packages can obtain the same results within the range of experimental errors when they use the same aperture size in processing. However, the aperture diameters determined by the two software packages are not equal, which would lead to a difference in the final results. The IRAF Apphot package commonly calculates the averaged full width at half maximum (FWHM) from many stars in the star pictures first and then uses 1.5 times the FWHM as the measuring aperture. SExtractor uses the growth curve method to compute the appropriate aperture. Considering the image integration of 300 seconds and atmospheric turbulence, the diameter of the observed star is bigger than that of the real one. Therefore, we can preliminarily predict that the growth curve method would be more stable and accurate.

Table 1 The g, r, i Observational Data for 3C 454.3

JD +2457600 (1)	$m_g \pm \sigma_g$ mag (2)	$m_r \pm \sigma_r$ mag (3)	$m_i \pm \sigma_i$ mag (4)
84.969	16.151±0.012	15.740±0.046	15.421±0.013
84.975	16.130±0.009	15.773±0.047	15.419±0.021
84.978	16.153±0.004	15.767±0.047	15.426±0.023
84.982	16.111±0.013	15.715±0.035	15.376±0.031
84.985	16.153±0.001	15.732±0.045	15.418±0.038
84.989	16.157±0.008	15.738±0.045	15.420±0.027
84.992	16.171±0.014	15.783±0.043	15.460±0.029
84.996	16.183±0.020	15.769±0.042	15.468±0.020
84.999	16.170±0.015	15.779±0.043	15.476±0.027
85.003	16.180±0.013	15.745±0.049	15.365±0.017
85.006	16.155±0.018	15.670±0.042	15.331±0.028
85.010	16.119±0.004	15.726±0.044	15.378±0.035
85.013	16.164±0.016	15.712±0.043	15.445±0.016
85.017	16.189±0.001	15.772±0.043	15.473±0.021
...	...	...	...
...	...	...	...
...	...	...	...

This table is available in its entirety in machine-readable and Virtual Observatory (VO) forms online at `http://www.raa-journal.org/docs/Supp/ms4385table1.xls`. A portion is shown here for guidance regarding its form and content.

3 RESULTS

3.1 Variation

When the data reduction process is applied to our simultaneous observations carried out with the NAGIOT during the period of 2016 Oct. 23 to Dec. 15, the magnitudes in g, r and i bands in 15 nights are obtained and listed in Table 1, in which Col. (1) gives JD (+2457600), Col. (2), g band, $m_g \pm \sigma_g$, Col. (3), r band, $m_r \pm \sigma_r$ and Col. (4), i band, $m_i \pm \sigma_i$. The corresponding light curves are depicted in Figure 1.

From Table 1, we know that there are 419 sets of observations for each band. The corresponding maximum variability amplitudes are $\Delta m_{g|\max} = 1.015 \pm 0.042$ mag, $\Delta m_{r|\max} = 1.188 \pm 0.050$ mag and $\Delta m_{i|\max} = 1.305 \pm 0.057$ mag.

IDV can occur when a light curve obeys the following requirements. (1) The optical variabilities (Δm) are not smaller than three times σ, $\Delta M \geq 3 \times \sigma$ (Fan et al. 2009a,b, 2014); (2) The variability parameter $C \geq 2.576$ (Romero et al. 1999); and/or (3) The F-test value is higher than the critical value (see Fan et al. 2018a).

During the 15 nights of observations, IDV was detected only on Nov. 2 (JD 2457694), and is plotted in Figure 2. We can see that the source brightness increases at first, and it then decreases. After a small bright state, it increases again at the g, r and i bands. At the g band, it brightens from $g = 15.440 \pm 0.030$ mag to $g = 15.277 \pm 0.026$ mag, which shows a variability of $\Delta g = -0.163 \pm 0.039$ mag (F = 22.76 while $F_{0.99} = 4.85$ and $F_{0.999} = 8.76$) over 50 min. The corresponding variability amplitude parameter (Heidt & Wagner 1996) $A_m = 15.8\%$. Then it decreases to $g = 15.506 \pm 0.039$ mag

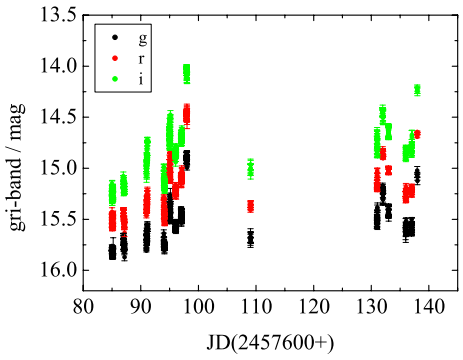

Fig. 1 The g, r, i light curves of our observations. The *black dots* stand for g band, the *red dots* for r band and the *green dots* for i band.

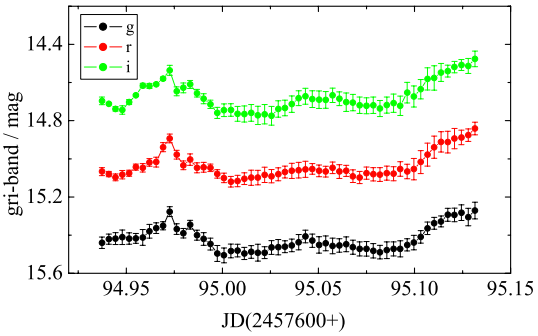

Fig. 2 The IDV light curve on Nov. 2 (JD 2457694). The *black dots* stand for g band, *red dots* represent r band and *green dots* signify i band.

($\Delta g = 0.229 \pm 0.046$ mag and $A_m = 22.5\%$, the corresponding $F = 29.03$, $F_{0.99} = 6.03$ and $F_{0.999} = 12$) over 40 min, afterwards a small bright state increasing from $g = 15.472 \pm 0.042$ to $g = 15.271 \pm 0.074$ mag ($\Delta g = -0.201 \pm 0.085$ mag and $A_m = 22.0\%$, $F = 18.02$, $F_{0.99} = 3.7$ and $F_{0.999} = 5.93$) over 55 min. At the r band, the variability and timescales are $\Delta r = -0.204 \pm 0.029$ mag ($A_m = 20.2\%$, $F = 62.15$, $F_{0.99} = 6.03$ and $F_{0.999} = 12$) over 40 min, $\Delta r = 0.227 \pm 0.036$ mag ($A_m = 22.4\%$, $F = 63.5$, $F_{0.99} = 5.31$ and $F_{0.999} = 10.0$) over 45 min, and $\Delta r = -0.212 \pm 0.050$ mag ($A_m = 20.6\%$, $F = 12.84$, $F_{0.99} = 3.231$ and $F_{0.999} = 4.9$) over 55 min. While at the i band, we have $\Delta i = -0.208 \pm 0.033$ mag ($A_m = 20.5\%$, $F = 19.85$, $F_{0.99} = 6.94$ and $F_{0.999} = 14.9$) over 35 min, $\Delta i = 0.228 \pm 0.046$ mag ($A_m = 22.3\%$, $F = 70.2$, $F_{0.99} = 4.85$ and $F_{0.999} = 8.76$) over 50 min, and $\Delta i = -0.246 \pm 0.065$ mag ($A_m = 23.7\%$, $F = 25.55$, $F_{0.99} = 3.7$ and $F_{0.999} = 5.93$) over 55 min.

3.2 Relationship Between Brightness and Color Indices

To analyze the relations between brightness and color indices, firstly, we apply the Galactic extinction correction using $A_g = 0.348$ mag, $A_r = 0.241$ mag and $A_i = 0.179$ mag from NED. We obtain 419 color indices in the form $g - r$, $g - i$ and $r - i$. $g - r$ is in the range of 0.190 ± 0.053 mag to 0.482 ± 0.036 mag with an average value of $\langle g - r \rangle = 0.345 \pm 0.052$ mag; $g - i$ is in the range of 0.482 ± 0.101 mag to 0.918 ± 0.056 mag with $\langle g - i \rangle = 0.706 \pm 0.096$ mag; and $r - i$ is in the range from 0.174 ± 0.054 mag to 0.574 ± 0.041 mag with $\langle r - i \rangle = 0.360 \pm 0.069$ mag.

When linear regression is adopted to analyze the color index and magnitude, the following results are obtained, $r - i = -(0.141 \pm 0.007)g + (2.591 \pm 0.113)$ with a correlation coefficient $r = -0.537$ and a chance probability of $p = 1.28 \times 10^{-37}$ as shown in Figure 3 (left panel); $g - i = -(0.249 \pm 0.006)r + (4.501 \pm 0.097)$ with $r = -0.758$ and $p = 3.08 \times 10^{-91}$, see Figure 3 (right panel); $g - r = -(0.119 \pm 0.006)i + (2.114 \pm 0.089)$ with $r = -0.743$ and $p = 4.41 \times 10^{-58}$, see Figure 3 (middle panel).

3.3 Period Analysis

Blazars sometimes manifest quasi-periodicity in their light curves. However, it is not easy to investigate periodicity in their light curves because the observations are not evenly sampled. Fortunately, there are some periodogram methods for unevenly sampled time series. In the present work, we will introduce the following methods: Power Spectrum Analysis (PSA), Jurkevich Method (JUR) and Discrete Correlation Function (DCF), and employ them for our Nov. 2 observations for periodicity investigation.

Power Spectrum Analysis (PSA): The most commonly used periodicity analysis is the periodogram method, which is an estimator of the signal energy in the frequency domain (Deeming 1975). Lomb (1976) introduced a modified form of this method, which is described as follows. If a series $x(n)$ has N points, let f be the frequency and τ be a variable timescale. Then the mean and standard deviation are given by: $\overline{x} = \frac{1}{N}\sum_{n=1}^{N} x(n)$ and $\sigma^2 = \frac{1}{N}\sum_{n=1}^{N}(x(n) - \overline{x})^2$ respectively. A normalized Lomb's P^L, i.e., the power spectrum as a function of angular frequency $\omega \equiv 2\pi f > 0$ is defined as

$$P_N^L(\omega) = \frac{1}{2\sigma^2}\left[\frac{[\sum_{n=0}^{N-1}(x(n) - \overline{x})\cos\omega(t_n - \tau)]^2}{\sum_{n=0}^{N-1}\cos^2\omega(t_n - \tau)}\right] + \frac{1}{2\sigma^2}\left[\frac{[\sum_{n=0}^{N-1}(x(n) - \overline{x})\sin\omega(t_n - \tau)]^2}{\sum_{n=0}^{N-1}\sin^2\omega(t_n - \tau)}\right], \quad (1)$$

and τ is defined by the equation

$$\tau(2\omega\tau) = \frac{\sum_{n=0}^{N-1}\sin 2\omega t_n}{\sum_{n=0}^{N-1}\cos 2\omega t_n}. \quad (2)$$

Jurkevich Method (JUR): JUR is based on the expected mean deviation. This tests a run of trial periods. For a trial period, p, all the data are folded using the trial period, then the folded data are assigned to m groups. For the

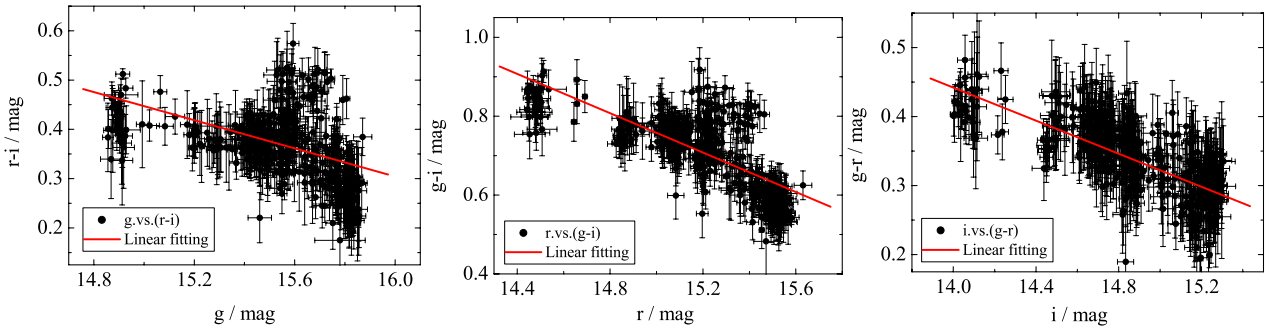

Fig. 3 The relations between brightness and color indices. The *solid lines* delineate the best linear fitting results.

ith (i = 1, 2, 3, ..., m) group, a deviation can be calculated, then one can acquire a total deviation, V_m^2, for the trial period. Therefore, we can get a series of V_m^2 corresponding to a series of trial periods. If the trial period is equal to the true one, then V_m^2 reaches a minimum. A 'good' period will return a much reduced variance relative to those produced by 'false' trial periods which have almost constant values. The error in the period can be estimated by calculating the FWHM of the minimum in V_m^2 (Jurkevich et al. 1971).

Discrete Correlation Function (DCF): The DCF method (Edelson & Krolik 1988; Hufnagel & Bregman 1992) is a method for exploring the correlation between two variable temporal sets with a given time lag. If we only apply the method to one set, then we can investigate the period of the set (Fan & Lin 2000). In order to execute this method, firstly we calculate the unbinned correlation (UDCF) of the two data streams a and b, i.e.,

$$\mathrm{UDCF}_{ij} = \frac{(a_i - \langle a \rangle) \times (b_j - \langle b \rangle)}{\sqrt{\sigma_a^2 \times \sigma_b^2}}, \qquad (3)$$

with a_i and b_j being two data streams, $\langle a \rangle$ and $\langle b \rangle$ being the average values of the data sets, and σ_a and σ_b being the corresponding standard deviation. Secondly, we average the points through sharing the same time lag by binning the UDCF_{ij} in suitably sized time-bins to compute the DCF for each time lag τ,

$$\mathrm{DCF}(\tau) = \frac{1}{M} \sum \mathrm{UDCF}_{ij}(\tau), \qquad (4)$$

where M is the total number of sets. The standard error of each bin is expressed as

$$\sigma(\tau) = \frac{1}{M} (\sum [\mathrm{UDCF}_{ij} - \mathrm{DCF}(\tau)]^2)^{0.5}. \qquad (5)$$

On 2016 Nov. 2, we monitored the sources in g, r and i bands, which yielded dense data. We implement PSA, DCF and JUR for our g, r and i observations, and retrieve the following periodicity analysis results, which are depicted in Figure 4.

At the g band, there are signs of two periodicities, $P_{g|1} = 109.36 \pm 17.53$ (PSA), 109.15 ± 13.08 (JUR) and 97.02 ± 18.17 (DCF) min, $P_{g|2} = 206.42 \pm 26.24$ (JUR), $P_{g|2} = 219.42 \pm 23.63$ (DCF) min.

Table 2 Periodicity analysis results at g, r, i bands on 2016 Nov. 2 for FSRQ 3C 454.3

Band	PSA (min)	JUR (min)	DCF (min)
g	109.36 ± 17.53	109.15 ± 13.08 206.42 ± 26.24	97.02 ± 18.78 219.42 ± 23.63
r	105.76 ± 12.08	111.4 ± 9.85 207.55 ± 30.59	106.67 ± 19.88 216.72 ± 23.52
i	101.47 ± 13.83	101.86 ± 10.13 190.61 ± 19.15	102.25 ± 27.80 197.62 ± 19.88

At r and i bands, we get similar results as listed in Table 2. So, the periodicities at g, r and i bands are $< P_g >= 105.06 \pm 28.83$ min, $< P_r >= 107.94 \pm 25.26$ min and $< P_i >= 101.86 \pm 32.69$ min, respectively.

4 DISCUSSION AND CONCLUSION

3C 454.3 is a well studied γ-ray bright source, which displays variabilities through all electromagnetic wavebands.

In this work, we report 15 nights of simultaneous g, r and i photometric observations carried out on the 1.26 m NAGIOT at Xinglong Station, NAOC for the FSRQ 3C 454.3 during the period of 2016 Oct. 23 to Dec. 15. There are 419 sets of observations at each band.

4.1 Variation

Our monitoring results suggest that the largest amplitude variations in the g, r and i bands are $\Delta m_{g|\max} = 1.015 \pm 0.042$ mag, $\Delta m_{r|\max} = 1.188 \pm 0.050$ mag and $\Delta m_{i|\max} = 1.305 \pm 0.057$ mag, respectively. Our maximum amplitude is smaller than $\Delta m = 2.3$ reported by Angel & Stockman (1980). Our monitoring result suggests that the variability amplitude at the longer waveband is larger than that in the shorter waveband.

IDV of blazars has been studied in many papers (Dai et al. 2009; Fan et al. 2009a,b,c, 2014; Gupta et al. 2008; Poon et al. 2009; Gaur et al. 2012). The origin of short timescales is probably produced in the innermost part of the accretion disk, which is very close to the central black hole. So, the short-term variance can be used to determine the black hole masses, rotation state of the central black hole and so on (Abramowicz & Nobili 1982;

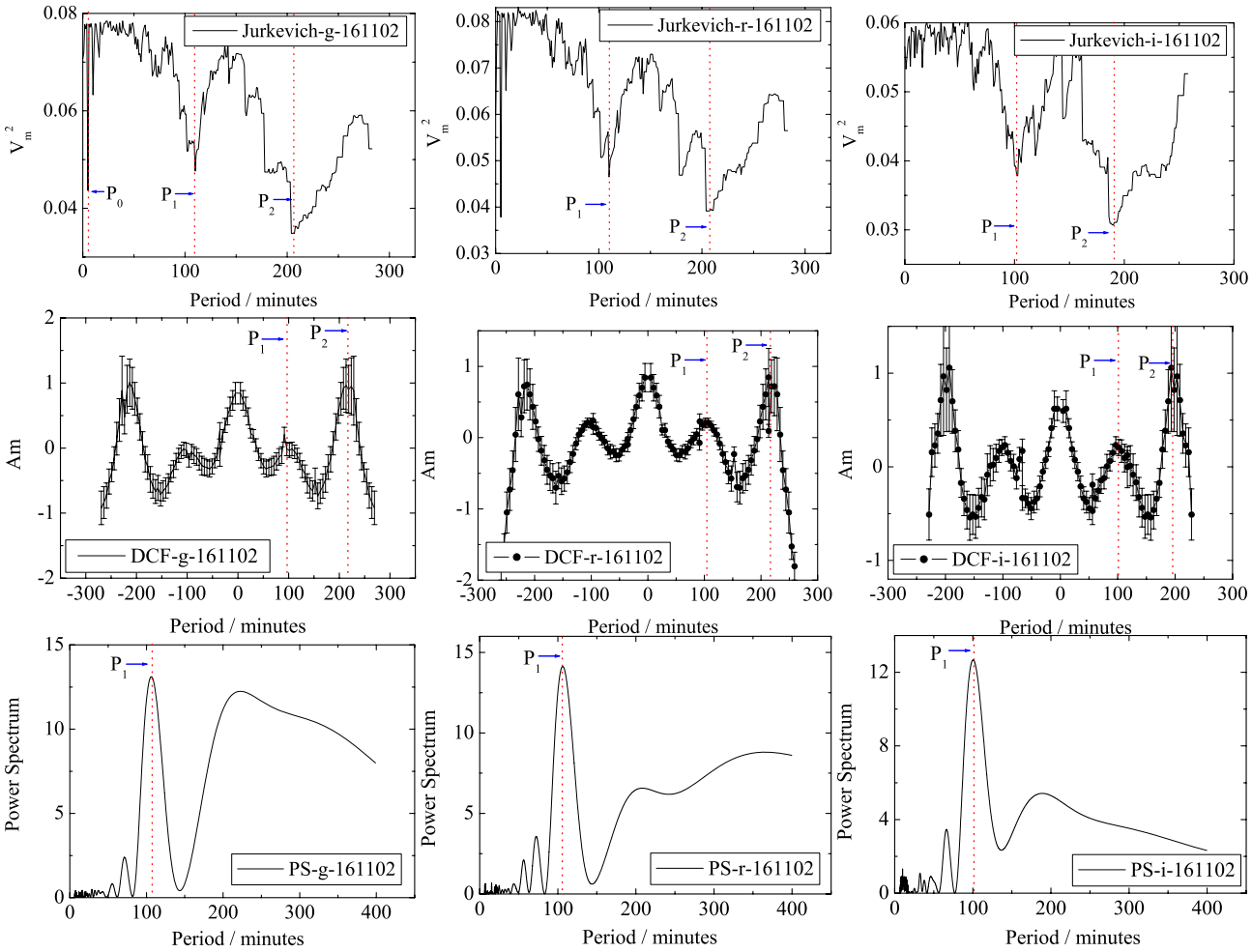

Fig. 4 Intra-day periodicity analysis results using JUR (*upper panels*), the DCF method (*middle panels*) and PSA (*bottom panels*). The *dotted lines* signify likely periodicities.

Miller et al. 1989). IDV is not a common phenomenon for this source. During the period of Oct. 2000, we monitored the source with the 70 cm telescope at Abastumani Observatory, Georgia, but we did not detect any IDV. During the present monitoring period, we only detected IDV on 2016 Nov. 2. The timescales are 35 min with a variability amplitude of $A_m = 20.5\%$ at i band to 55 min with a variability amplitude of $A_{m|r} = 20.59\% \sim A_{m|i} = 23.71\%$.

The observations on Nov. 2 display signs of IDV periodicities. In that day, the total monitored time is about 4.6 h. Our period analyses give $< P_g >= 105.06 \pm 28.83$ min, $< P_r >= 107.94 \pm 25.26$ min and $< P_i >= 101.86 \pm 32.69$ min. The weighted average value is $< p >= 105.88$ min. Our analysis also hints of $p_2 \sim 200$ min period in the JUR and DCF analysis methods, $P_2 \sim 2P_1$. So, P_2 is possibly a harmonic of P_1. Actually, from Figure 2, we can see that the source becomes bright at first, and it then becomes faint. Afterwards, its brightness increases and then it becomes faint. Finally, it becomes bright again. The time interval between the first bright peak and the small peak is $100 \sim 110$ min, and that between the small peak and the 2nd brightness peak is $116 \sim 128$ min. The derived period of 105 min is consistent with the time intervals.

4.2 Central Black Hole Mass

If the IDV period indicates the period of the innermost stable circular orbit, then an upper limit can be obtained for the central black hole mass. The innermost stable circular orbit depends on properties of the black hole and accretion disk (Fan 2005, see also Fan et al. 2014).

- $r = \frac{6GM}{c^2}$ for a thin accretion disk surrounding a Schwarzschild black hole;
- $r = \frac{4GM}{c^2}$ for a thick accretion disk surrounding a Schwarzschild black hole;
- $r = 1.48 \times 10^5 (1 + \sqrt{1 - a^2}) \frac{M}{M_\odot}$, here r is the radius of the event horizon of a Kerr black hole with mass M and angular momentum parameter a.

If we take the period p as the time for the light to travel in the innermost stable circular orbit, then $2\pi r = cp\delta/(1+z)$, where δ is a Doppler factor, so we have

- $M = 3.18 \times 10^5(\frac{\delta}{1+z})(\frac{p}{1\mathrm{min}})M_\odot$ for a thin accretion disk surrounding a Schwarzschild black hole;
- $M = 4.77 \times 10^5(\frac{\delta}{1+z})(\frac{p}{1\mathrm{min}})M_\odot$ for a thick accretion disk surrounding a Schwarzschild black hole;
- $M = 1.93 \times 10^6(\frac{\delta}{1+z})(\frac{p}{1\mathrm{min}})M_\odot$ for an extreme Kerr black hole with angular momentum parameter $a = 1$.

For 3C 454.3, $z = 0.859$ and $p = 105.88$ min and if $\delta = 17.0$ (Liodakis et al. 2017) is adopted, we can calculate the mass of the black hole $M = (0.30 \sim 1.85) \times 10^9\, M_\odot$.

The central black hole mass is estimated using different methods for the source. Gu et al. (2001) estimated $M = 4.41 \times 10^9\, M_\odot$ using $M = R_{\mathrm{BLR}}V^2/G$, Woo & Urry (2002) avail the optical luminosity to calculate the black hole mass and get $M = 1.49 \times 10^9\, M_\odot$, Bonnoli et al. (2011) estimated a mass of $M = (0.34 \sim 1.2) \times 10^9\, M_\odot$, Sbarrato et al. (2012) obtained $\sim 5.01 \times 10^9\, M_\odot$ while Gupta et al. (2017) reported $(2.3 \pm 0.5) \times 10^9 M_\odot$ for the black hole mass. Our estimations are consistent with theirs.

4.3 Relationship Between Brightness and Color Indices

Blazars exhibit different phenomena concerning the relationship between color index and magnitude, which have been discussed in many papers (Edelson et al. 1990; Trèvese & Vagnetti 2002; Vagnetti et al. 2003; Gu et al. 2006; Dai et al. 2009; Poon et al. 2009; Yuan et al. 2015a; Yuan et al. 2015b). Generally, BL Lacs show that the spectrum generally becomes blue when the source becomes bright (bluer when brighter, BWB), and they become red when the source becomes faint. For FSRQs, there is a complicated relation between the color index and magnitude. Some FSRQs manifest a red spectrum that corresponds to a bright state (redder when brighter, RWB), some exhibit a similar phenomenon to BL Lacs, while others show both BWB and RWB behaviors.

In the present work, 3C 454.3 manifests a strong anti-correlation between the g, r, i magnitudes and color indices. This means that when the source becomes brighter the spectrum become redder, which is a common phenomenon in FSRQs. The RWB behavior of 3C 454.3 is also discussed in a paper by Zhou et al. (2015). The RWB in 3C 454.3 is also consistent with the larger variation amplitude at longer wavelengths found in the present work.

4.4 Conclusions

In this paper, we present simultaneous photometry observations of the FSRQ 3C 454.3 and provide the following analysis results:

1. The maximum variabilities are $\Delta m_{g|\mathrm{max}} = 1.015 \pm 0.042$ mag, $\Delta m_{r|\mathrm{max}} = 1.188 \pm 0.050$ mag and $\Delta m_{i|\mathrm{max}} = 1.305 \pm 0.057$ mag.

2. During our observations, IDVs are detected only on one night, with timescales from 35 to 55 min. There is a period of 105.88 min in the g, r, i light curves, which suggests the mass of the central black hole $M = (0.30 \sim 1.85) \times 10^9\, M_\odot$.

3. There is an anti-correlation between the color index and magnitude, suggesting that it becomes redder when it brightens.

Acknowledgements The work is partially supported by the National Natural Science Foundation of China (Grant Nos. U1531245, 11733001, U1831119, 11873073, 11173009, U1431112, 11733006 and 11873073), the Natural Science Foundation of Guangdong Province (2017A030313011), supports for Astrophysics Key Subjects of Guangdong Province and Guangzhou City, and Science and Technology Program of Guangzhou (201707010401). The authors thank the referee for good suggestions! The Galactic Extinction value comes from `http://ned.ipac.caltech.edu/`.

References

Abramowicz, M. A., & Nobili, L. 1982, Nature, 300, 506
Ackermann, M., Ajello, M., Atwood, W. B., et al. 2015, ApJ, 810, 14
Ahn, C. P., Alexandroff, R., Allende Prieto, C., et al. 2012, ApJS, 203, 21
Angel, J. R. P., & Stockman, H. S. 1980, ARA&A, 18, 321
Bennett, A. S. 1962, MmRAS, 68, 163
Bennett, C. L., Hill, R. S., Hinshaw, G., et al. 2003, ApJS, 148, 97
Bertin, E., & Arnouts, S. 1996, A&AS, 117, 393
Blandford, R. D., & Rees, M. J. 1978, in BL Lac Objects, ed. A. M. Wolfe, 328
Blom, J. J., Bloemen, H., Bennett, K., et al. 1995, A&A, 295, 330
Bonnoli, G., Ghisellini, G., Foschini, L., et al. 2011, MNRAS, 410, 368
Britto, R. J., Bottacini, E., Lott, B., et al. 2016, ApJ, 830, 162
Cellone, S. A., Romero, G. E., & Combi, J. A. 2000, AJ, 119, 1534
Chakrabarti, S. K., & Wiita, P. J. 1993, ApJ, 411, 602
Dai, B. Z., Li, X. H., Liu, Z. M., et al. 2009, MNRAS, 392, 1181
de Diego, J. A. 2010, AJ, 139, 1269
de Diego, J. A. 2014, AJ, 148, 93
de Diego, J. A., Polednikova, J., Bongiovanni, A., et al. 2015, AJ, 150, 44
Deeming, T. J. 1975, Ap&SS, 36, 137
Edelson, R. A., & Krolik, J. H. 1988, ApJ, 333, 646
Edelson, R. A., Krolik, J. H., & Pike, G. F. 1990, ApJ, 359, 86
Fan, J.-H. 2005, ChJAA (Chin. J. Astron. Astrophys.), 5S, 213

Fan, J. H., Cheng, K. S., & Zhang, L. 2001, PASJ, 53, 201
Fan, J.-H., Kurtanidze, O. M., Nikolashvili, M. G., et al. 2004, ChJAA (Chin. J. Astron. Astrophys.), 4, 133
Fan, J. H., Zhang, Y. W., Qian, B. C., et al. 2009a, ApJS, 181, 466
Fan, J. H., Peng, Q. S., Tao, J., et al. 2009b, AJ, 138, 1428
Fan, J.-H., Yuan, Y.-H., Liu, Y., et al. 2009c, RAA (Research in Astronomy and Astrophysics), 9, 538
Fan, J. H., & Lin, R. G. 2000, ApJ, 537, 101
Fan, J. H., Kurtanidze, O., Liu, Y., et al. 2014, ApJS, 213, 26
Fan, J. H., Yang, J. H., Liu, Y., et al. 2016, ApJS, 226, 20
Fan, J. H., Kurtanidze, O., Liu, Y., et al. 2017a, ApJ, 837, 45
Fan, J. H., Yang, J. H., Xiao, H. B., et al. 2017b, ApJ, 835, L38
Fan, J. H., Tao, J., Liu, Y., et al. 2018, AJ, 155, 90
Fuhrmann, L., Cucchiara, A., Marchili, N., et al. 2006, A&A, 445, L1
Gaia Collaboration, Brown, A. G. A., Vallenari, A., et al. 2016, A&A, 595, A2
Gaur, H., Gupta, A. C., & Wiita, P. J. 2012, AJ, 143, 23
Ghisellini, G., Tavecchio, F., Foschini, L., et al. 2011, MNRAS, 414, 2674
Ghisellini, G., & Tavecchio, F. 2015, MNRAS, 448, 1060
Giommi, P., Blustin, A. J., Capalbi, M., et al. 2006, A&A, 456, 911
Gu, M., Cao, X., & Jiang, D. R. 2001, MNRAS, 327, 1111
Gu, M. F., Lee, C.-U., Pak, S., et al. 2006, A&A, 450, 39
Gupta, A. C., Fan, J. H., Bai, J. M., et al. 2008, AJ, 135, 1384
Gupta, A. C., Mangalam, A., Wiita, P. J., et al. 2017, MNRAS, 472, 788
Hartman, R. C., Bertsch, D. L., Dingus, B. L., et al. 1993, ApJ, 407, L41
Hartman, R. C., Bertsch, D. L., Bloom, S. D., et al. 1999, ApJS, 123, 79
Heidt, J., & Wagner, S. J. 1996, A&A, 305, 42
Hufnagel, B. R., & Bregman, J. N. 1992, ApJ, 386, 473
Jackson, N., & Browne, I. W. A. 1991, MNRAS, 250, 414
Jorstad, S. G., Marscher, A. P., Smith, P. S., et al. 2013, ApJ, 773, 147
Jurkevich, I., Usher, P. D., & Shen, B. S. P. 1971, Ap&SS, 10, 402
Kurtanidze, O. M., Tetradze, S. D., Richter, G. M., et al. 2009, in Astronomical Society of the Pacific Conference Series, 408, The Starburst-AGN Connection, eds. W. Wang, Z. Yang, Z. Luo, & Z. Chen, 266
Kushwaha, P., Gupta, A. C., Misra, R., & Singh, K. P. 2017, MNRAS, 464, 2046
Lin, C., & Fan, J.-H. 2018, RAA (Research in Astronomy and Astrophysics), 18, 120
Liodakis, I., Marchili, N., Angelakis, E., et al. 2017, MNRAS, 466, 4625
Liu, X., Yang, P. P., Liu, J., et al. 2017, MNRAS, 469, 2457
Lloyd, C. 1984, MNRAS, 209, 697
Lomb, N. R. 1976, Ap&SS, 39, 447
Mangalam, A. V., & Wiita, P. J. 1993, ApJ, 406, 420
Marscher, A. P., & Gear, W. K. 1985, ApJ, 298, 114
Meng, N., Zhang, X., Wu, J., Ma, J., & Zhou, X. 2018, ApJS, 237, 30
Miller, H. R., Carini, M. T., & Goodrich, B. D. 1989, Nature, 337, 627
Mommert, M. 2017, Astronomy and Computing, 18, 47
Pandey, A., Gupta, A. C., Wiita, P. J., & Tiwari, S. N. 2019, ApJ, 871, 192
Pei, Z.-Y., Fan, J.-H., Bastieri, D., Sawangwit, U., & Yang, J.-H. 2019, RAA (Research in Astronomy and Astrophysics), 19, 070
Pian, E., Foschini, L., Beckmann, V., et al. 2006, A&A, 449, L21
Poon, H., Fan, J. H., & Fu, J. N. 2009, ApJS, 185, 511
Raiteri, C. M., Ghisellini, G., Villata, M., et al. 1998, A&AS, 127, 445
Rieger, F. 2019, Galaxies, 7, 28
Romero, G. E., Cellone, S. A., & Combi, J. A. 1999, A&AS, 135, 477
Sandage, A. 1966, ApJ, 144, 1234
Sbarrato, T., Ghisellini, G., Maraschi, L., & Colpi, M. 2012, MNRAS, 421, 1764
Stickel, M., Padovani, P., Urry, C. M., et al. 1991, ApJ, 374, 431
Tao, J., Fan, J., Qian, B., & Liu, Y. 2008, AJ, 135, 737
Tavecchio, F., Maraschi, L., Ghisellini, G., et al. 2002, ApJ, 575, 137
Trèvese, D., & Vagnetti, F. 2002, ApJ, 564, 624
Urry, C. M., & Padovani, P. 1995, PASP, 107, 803
Vagnetti, F., Trevese, D., & Nesci, R. 2003, ApJ, 590, 123
Vercellone, S., D'Ammando, F., Vittorini, V., et al. 2010, ApJ, 712, 405
Villata, M., Raiteri, C. M., Balonek, T. J., et al. 2006, A&A, 453, 817
Wagner, S. J., & Witzel, A. 1995, ARA&A, 33, 163
Woo, J.-H., & Urry, C. M. 2002, ApJ, 579, 530
Worrall, D. M., Giommi, P., Tananbaum, H., et al. 1987, ApJ, 313, 596
Xiao, H. B., Fan, J. H., Yang, J. H., et al. 2019, SCMPA (Science China Physics, Mechanics, and Astronomy), 62, 129811
Xiong, D., Bai, J., Zhang, H., et al. 2017, ApJS, 229, 21
Yang, J. H., Fan, J. H., Zhang, Y. I., et al. 2018a, Acta Astronomica Sinica, 59, 38
Yang, J., Fan, J., Liu, Y., et al. 2018b, SCMPA (Science China Physics, Mechanics, and Astronomy), 61, 59511
Yuan, Y. H., Fan, J. H., & Pan, H. J. 2015a, AJ, 150, 67
Yuan, Y. H., Fan, J. H., Pan, H. J., et al. 2015b, Ap&SS, 360, 9
Zhang, S., Collmar, W., & Schönfelder, V. 2005, A&A, 444, 767
Zhang, X., Wu, J., & Meng, N. 2018, MNRAS, 478, 3513
Zhou, Y., Yan, D.-H., & Dai, B.-Z. 2015, New Astron., 36, 19